RESEARCH ARTICLE

Feasibility of Active Reactance Compensator for Autonomously Maximizing Repeater Coil Current of Wireless Power Transfer System Against Variations in Resonant Frequency and Magnetic Coupling Intensity

MASATAKA ISHIHARA[ID][1]**, (Member, IEEE), KAZUHIRO UMETANI**[ID][1]**, (Member, IEEE), AKIHIRO KONISHI**[ID][2]**, (Member, IEEE), AND EIJI HIRAKI**[ID][1]**, (Member, IEEE)**
[1]Faculty of Life, Environment, Natural Science and Technology, Okayama University, Okayama 700-8530, Japan
[2]Graduate School of Science and Engineering, Chiba University, Chiba 263-8522, Japan

Corresponding author: Masataka Ishihara (masataka.ishihara@okayama-u.ac.jp)

ABSTRACT In resonant inductive coupling wireless power transfer systems, a repeater resonator is crucial in expanding the charging area, enabling efficient power supply to receivers, such as small Internet of Things (IoT) devices sparsely distributed in a wide area. However, the repeater current is highly susceptible to deviations in resonance frequency due to manufacturing tolerance and aging, as well as to the magnetic coupling between the transmitter and repeater coils, potentially leading to insufficient amplitude. Consequently, the magnetic field generated by the repeater decreases and the receiver may be difficult to obtain sufficient power from the transmitter via the repeater. To address this problem, this paper proposes a wireless power transfer system with active reactance compensators incorporated in the repeater and the transmitter. The proposed system can equivalently adjust the resonant frequencies of the transmitter and repeater to stably maximize the repeater coil current regardless of the variations in the resonant frequency and the magnetic coupling intensity. Experiments successfully verify that the proposed system can provide a more stable and larger repeater current and output power than the conventional system against the variations in the magnetic field intensity and the resonant frequency of the repeater, validating the feasibility of the proposed system for practical utilization of the repeater in expanding the charging area.

INDEX TERMS Resonant inductive coupling, wireless power transfer, repeater, intermediate resonator, frequency splitting phenomenon.

I. INTRODUCTION

Recently, wireless power transfer (WPT) techniques have been gaining increasing attention as a key technology for Internet of Things (IoT) proliferation [1], [2], [3], [4].

The associate editor coordinating the review of this manuscript and approving it for publication was Khaled Ahmed[ID].

WPT techniques can supply electric power without physical cable connections, thus realizing convenient, reliable, and safe power supplies. This is advantageous as a power supply method to multiple IoT devices (e.g., active radio frequency identification tags, electronic shelf labels, and smart sensors) dispersed in a wide area. Traditional power methods, like internal batteries, have limitations in operation time and space

requirements [2], [3], [4], [5]. The WPT technique can offer a solution to these problems.

A resonant inductive coupling WPT (RIC-WPT) technique is promising in efficiently powering multiple IoT devices over wide areas [2], [6]. Generally, RIC-WPT systems for powering multiple IoT devices comprise a transmitter and receivers (Fig. 1). The transmitter with an inverter excites a resonance in the receiver via magnetic coupling. Usually, the resonators of the receivers are designed to have the same resonant frequency as the operating frequency of the transmitter to ensure effective resonance in the receiver [4], [5].
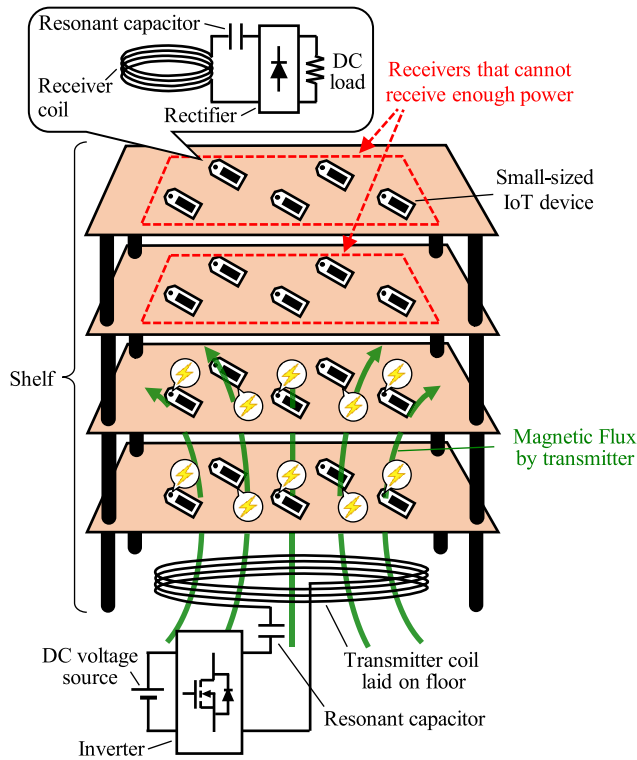

FIGURE 1. Typical RIC-WPT system without repeater for powering small-sized IoT devices.

However, the RIC-WPT system still suffers from insufficient power transfer capability to charge the IoT devices in a wide area. The transmitter's magnetic flux density diminishes with distance, and receiver coils are often small due to space constraints, leading to reduced power transfer [1], [7]. Introducing a repeater (Fig. 2), comprising a coil and resonant capacitor, can address this problem. The resonance current in the repeater generates a magnetic field around the repeater coil, expanding the charging area for the receivers [1], [7], [8], [9], [10], [11], [12], [13], [14]. Since the repeater is physically separated from the transmitter, it can be placed in the desired location. Therefore, inserting a repeater may be reasonable because the repeater can expand the charging area based on the location of small-sized receivers dispersed in a wide area.

Precise frequency tuning is crucial for repeater efficacy. Deviations in the repeater's resonant frequency from the operating frequency due to manufacturing tolerance or aging can
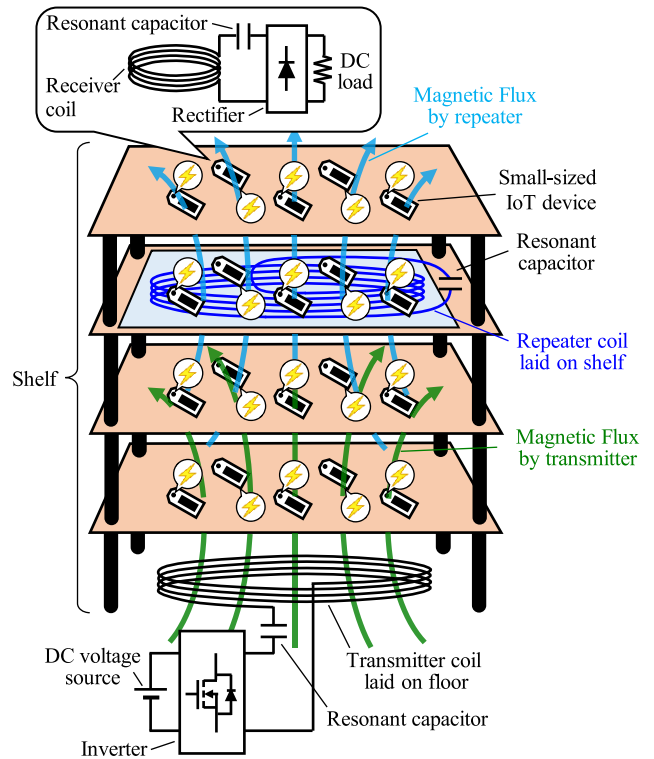

FIGURE 2. Typical RIC-WPT system with repeater for powering small-sized IoT devices.

reduce effectiveness. Because the repeater has no power load, the quality factor of the repeater resonator is so large. Therefore, a slight detuning can significantly reduce the resonant current of the repeater, leading to a significant reduction in the receiver's output power. Frequency splitting, a phenomenon where optimal frequencies can split into multiple sub-peak frequencies under strong magnetic coupling, also poses challenges [8], [9], [10], [11], [12], [13], [14]. These frequencies slightly deviate from the resonant frequency of the repeater depending on the magnetic coupling intensity.

Similar problems also occur in the receiver of the RIC-WPT systems, but the impact on power transfer is less due to the receiver's lower quality factor. Nonetheless, the frequency adjustment of the RIC-WPT system has been conventionally targeted at the receiver based on a basic two-coil RIC-WPT system, comprising a transmitter and a receiver [15], [16], [17], [18], [19], [20], [21]. For example, [15], [16], [17] adopted a passive approach, optimizing the coupling coefficient between coils to maximize receiver current and avoid frequency splitting. However, this limited the repeater's positioning flexibility and made it difficult to cope with the manufacturing tolerance and the aging effect. Meanwhile, [18], [19], [20] dynamically controlled the operating frequency of the transmitter in search of the maximum current induction in the receiver. However, this required a high voltage power supply to the inverter to have a sufficient controllable operating frequency range with a sufficient amplitude of the transmitter coil current because of

the high-quality factor of the transmitter resonator. To overcome this difficulty, some studies have proposed actively adjusting resonant frequencies through mechanical [21] or electrical [12], [13], [14], [22], [23], [24], [25], [26], [27], [28], [29] variation of resonant capacitance. These studies successfully adjusted the resonant frequency. However, these achievements are still faced with the difficulty in constructing practical WPT systems that can stably and autonomously adjust the resonant frequency owing to the lack of a practical implementation method for these techniques, including their autonomous control method.

The purpose of this paper is to propose a WPT system that can stably maximize the repeater resonator current against the manufacturing tolerance, aging effect, and variation in magnetic coupling. The proposed system utilizes the active reactance compensator, referred to as the automatic tuning assist circuit (ATAC) [12], [13], [14], [28], [29]. The ATAC was first proposed in a previous study [28] as a dynamic variable capacitor to adjust the resonant frequency of the transmitter. The proposed system includes the ATACs on the both the transmitter and repeater to equivalently adjust the resonant frequency of the transmitter and repeater resonators. This paper further discusses the implementation and control strategy of this technique for a stable and autonomous adjustment of the resonant frequency to maximize the repeater current. Note that this paper focuses on low-power applications, such as those shown in Figure 1, where the output power of the receivers is low, and the magnetic field generated by the receivers is significantly smaller than that generated by the transmitter or repeater. Therefore, this paper can contribute to achieving a WPT system with a wide charging area for low-power applications such as IoT devices.

However, it should also be noted that this paper remains the elucidation of the feasibility of this novel proposed WPT system because two essential but not fundamental parts of the system are still under development for finally constructing the proposed WPT system: One is the wireless real-time communication circuit transferring the information on the phase angle of the transmitter coil current, and the other is the digital implementation of the autonomous resonant frequency control in the microprocessor. The performance of the proposed WPT system was tested through experiments by manually adjusting the phase angle to control the ATAC according to the predetermined control flow based on the information of the phase angle of the transmitter coil current transferred through the physically connected wire.

This paper is a continuation of the conference paper [12] and [13]. Based on [12] and [13], a detailed explanation of the overall system configuration and control flowchart of the proposed WPT system is provided in this study. Furthermore, an experiment showing the effective expansion of the charging area using the proposed WPT system was conducted.

The paper is structured as follows: Section II outlines the proposed WPT system and its operating principles. Section III details the control strategy. Sections IV report on experiments focusing on stabilizing the repeater coil current and expanding the charging area. Finally, section V provides a summary of this paper.

II. PROPOSED WIRELESS POWER TRANSFER SYSTEM
A. POWER CIRCUIT OVERVIEW

Fig. 3 shows the schematics of the power circuit of the proposed WPT system with a repeater, where W_1 and W_2 are the transmitter and repeater coils, respectively, v_{in} is the inverter output in the transmitter; S_1–S_4 are the switching devices; v_{A1} and v_{A2} are the output voltages of the ATACs; i_1 and i_2 are the transmitter and repeater currents. The power circuit of the proposed WPT system is constructed by adding the ATACs to the transmitter and repeater resonators of the WPT system shown in Fig. 2.
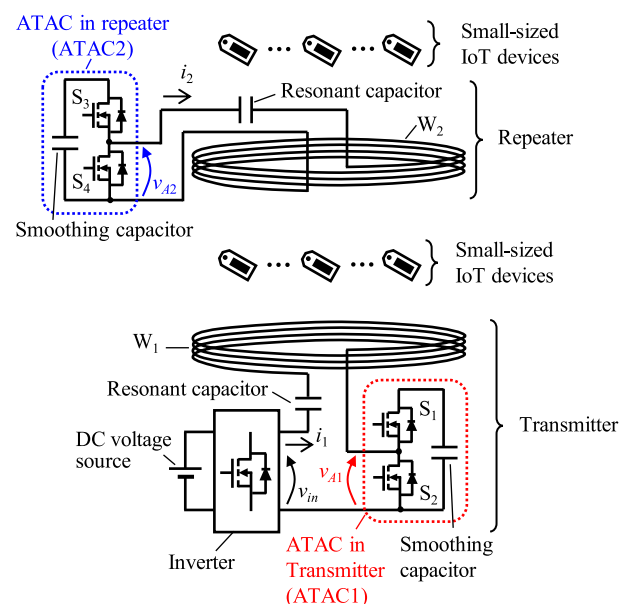

FIGURE 3. Power circuit of proposed WPT system.

The ATAC works as an equivalent variable capacitor to equivalently adjust the resonant frequency of the transmitter and repeater resonators. Among the various techniques to vary the resonant frequency, the ATAC was adopted owing to its simple control. Specifically, the ATAC in the transmitter depicted in Fig. 3 does not require any feedback control to maximize the repeater current stably and autonomously, as discussed in the subsequent two subsections. If another technique for varying the resonant frequency is employed on the transmitter side, it may require feedback on the phase difference between the inverter output voltage and transmitter current.

When there are multiple receivers, as shown in Fig. 3, the output power may decrease not only due to the deviation of the resonant frequency of the receivers but also because of cross-coupling among the receivers. Therefore, strictly speaking, to obtain a large output power, the resonant

frequency of the receiver should also be adjusted appropriately. However, adjusting the resonant frequency of the receiver is out of the scope of this paper. Usually, in the RIC-WPT for small-sized receivers with low-power applications, such as IoT devices, the resonant frequency detuning of the receiver will not pose a serious problem compared to that of the transmitter and repeater. The receiver is connected to a load, which lowers the quality factor of the resonator and has relatively little effect on the deviation of the resonant frequency. Furthermore, the effect of the cross-coupling among the receivers should be minimal in a low-power RIC-WPT system because the magnetic fields generated by the transmitter and repeater are typically much stronger than those generated by the small-sized receivers.

B. AUTOMATIC TUNING ASSIST CIRCUIT (ATAC)

The basic circuit diagram of the ATAC comprises only a half-bridge circuit and a smoothing capacitor, as shown in Fig. 3. The smoothing capacitor's capacitance significantly exceeds that of the resonant capacitors in the transmitter and repeater, maintaining nearly constant DC voltage despite the inflow of high-frequency resonant current into the ATAC.

The switching devices of the half-bridge circuit are operated alternately at the fixed duty ratio of 0.5 and at the same frequency as the ac current flowing into the ATAC. Thus, the only remaining freedom of operation lies in the phase angle of the gating signal of the half-bridge circuit. The operation of the ATAC is controlled by adjusting the phase angle difference between the gating signal and the ac voltage that drives the resonators of the transmitter or repeater, i.e., the inverter output voltage for the ATAC of the transmitter and the induced voltage in the repeater coil for the ATAC of the repeater. Consequently, the ATAC generates the square wave voltage of the operating frequency at the intermediate point of the half-bridge circuit, i.e., v_{A1} and v_{A2} defined in Fig. 3, with a phase difference to the ac voltage.

Next, the basic operation of the ATAC is discussed based on a simple LC resonator circuit shown in Fig. 4, representing the transmitter and repeater. The ac voltage (v_{ac} in Fig. 4) corresponds to the fundamental wave of the inverter output voltage in the transmitter and the fundamental wave of the induced voltage in the repeater. In this subsection, i_{ac} denotes the resonant current; v_A denotes the output voltage of the ATAC; S_{A1} and S_{A2} denote the switching devices of the ATAC.
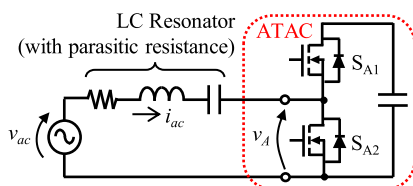
The ATAC is a lossless circuit with only two switching devices and a smoothing capacitor. Therefore, the ATAC appears as a reactance to the resonant current in the steady-state operation. Meanwhile, the phase angle of the square wave generated by the ATAC should be delayed from that of the ac current flowing into the ATAC to achieve the zero voltage switching (ZVS) turn-on of the ATAC. Consequently, the ATAC can be utilized in adding capacitance to the resonator.

Because the ATAC works as capacitance, the resonator is designed to be slightly inductive at the frequency of the ac voltage. This enables the adjustment of the equivalent resonant frequency of the entire circuit around the frequency of the ac voltage. We considered adjusting the phase angle difference φ between the gating signal of S_{A1} and the ac voltage. The phase angle difference φ, between the gating signal of SA1 and the AC voltage, is adjustable within the range $\lambda - \pi/2 \leq \varphi \leq 0$ (Fig. 5(a)), where λ is the phase angle of the LC resonator's admittance Y_{res}, excluding the ATAC.
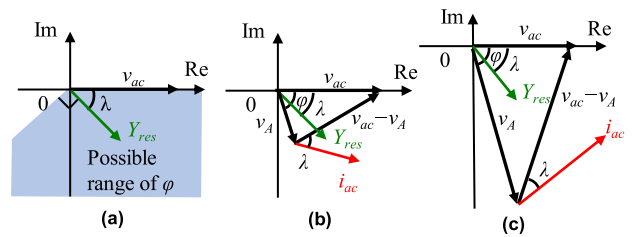

FIGURE 5. Phasor diagrams of Fig. 4. (a) Possible range of φ. (b) Smoothing capacitor voltage is smaller than that in steady state. (c) Smoothing capacitor voltage is greater than that in steady state.

Before reaching the steady state, the ATAC can receive or release the active power. The active power received and released by the ATAC results in the increase and decrease in the dc voltage of the smoothing capacitor, respectively. If the dc voltage in the smoothing capacitor is smaller than that in the steady-state operation, the ATAC receives the active power to increase the dc voltage because the product of v_A and i_{ac} is positive as shown in Fig. 5(b). Conversely, if the voltage of the smoothing capacitor is greater than that in the steady-state operation, the ATAC releases the active power to decrease the dc voltage because the product of v_A and i_{ac} is negative as shown in Fig. 5(c). Consequently, the ATAC autonomously reaches the steady state, where i_{ac} is perpendicular to v_{ac} to receive no active power.

In the steady state, i_{ac} has the phase angle difference of $\pi/2$ to the gate signal of S_{A1}. The phase angle difference θ of i_{ac} relative to v_{ac} can be controlled from λ to $\pi/2$ by adjusting φ. Because parasitic resistance in many LC resonators is small, λ is typically near $\pi/2$, allowing for θ control within the range of $-\pi/2$ to $\pi/2$. Notably, θ represents the phase angle of the equivalent impedance of the total LC resonator including the ATAC. Hence, controlling θ is equivalent to controlling the reactance of the equivalent impedance of the LC resonator. Particularly, by realizing $\theta = 0$, the reactance of

FIGURE 4. Simple series LC resonant circuit with ATAC.

the LC resonator is nullified, which is equivalent to tuning the resonant frequency to the frequency of the ac voltage source.

C. OPERATING PRINCIPLE

The proposed WPT system attaches the ATACs to the transmitter and repeater resonators. These ATACs are operated by adjusting the phase angle of their high-side switch to the ac power source generated by the inverter of the transmitter. This subsection theoretically discusses how the repeater coil current can be maximized regardless of the variations in the resonant frequency and magnetic coupling intensity by adjusting these phase angles.

As previously discussed, the ATAC equivalently works as a variable capacitor. Therefore, the proposed WPT system can be expressed using the equivalent circuit shown in Fig. 6, where L_1 and L_2 are the self-inductances of W_1 and W_2, respectively; C_1 and C_2 are the capacitances of the resonant capacitors; r_1 and r_2 are the series parasitic resistances of the transmitter and the repeater coils; M is the mutual inductance between W_1 and W_2; v_{ind} is the ac voltage induced in the repeater coil. The ATACs of the transmitter and repeater are expressed as the variable capacitors with reactance X_{A1} and X_{A2}, respectively.
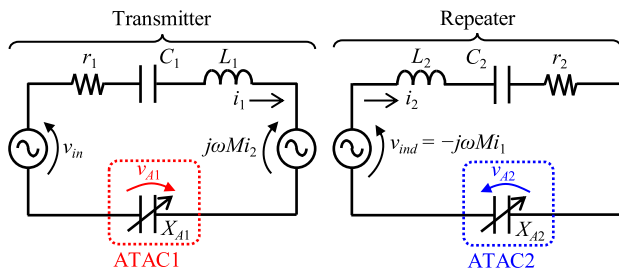

FIGURE 6. Simplified equivalent circuit of Fig. 3.

In this equivalent circuit, the receivers were omitted to simplify the analysis of the transmitter and repeater currents. In our intended low-power applications, as shown in Figure 1, the transmitter and repeater currents are typically little affected by the small-sized receiver because the electromotive force induced by the receivers in the transmitter and repeater is negligible due to the sufficiently small size of the receiver coils compared to those of the transmitter and repeater. Thus, this approximation is reasonable. Strictly speaking, the operation of the small receivers has a slight effect on the transmitter and repeater currents. This effect can be modeled as the reflected impedances [12], [13], [17] in the transmitter and repeater. Hence, the reflected impedances added by the receivers are assumed to be included in the parasitic resistance r_1 and r_2, as well as the coil inductance L_1 and L_2. In this sense, the coil parameters, i.e., r_1, r_2, L_1, and L_2, slightly vary not only by the manufacturing tolerance and the aging effect but also by the location of the receivers, the output power, and the resonant frequency of the receivers. Therefore, this discussion counts not only the manufacturing

tolerance and the aging effect but also the reactance of the reflected impedance of small-seized receivers for the variation of the resonant frequency.

Next, we analyzed the operation of the equivalent circuit. To simplify the analysis, the following discussion adopts the first harmonics approximation because the transmitter and repeater do not have the electric load and therefore the quality factors of their resonators are commonly far greater than 1.

The power consumed in the repeater resonator is proportional to the square of the amplitude of the repeater coil current i_2. Thus, to maximize the repeater current amplitude, the repeater power consumption must be maximized. The repeater circuit in Fig. 6 is transformed into the reflected impedance attached to the transmitter circuit, as shown in Fig. 7 to calculate the power consumption of the repeater resonator, where Z_{ref} is the reflected impedance. The real and imaginary parts of Z_{ref} are expressed as

$$\text{Re}\left(Z_{ref}\right) = \frac{\omega^2 M^2 r_2}{(X_2 + X_{A2})^2 + r_2^2}, \tag{1}$$

$$\text{Im}\left(Z_{ref}\right) = -\frac{\omega^2 M^2 (X_2 + X_{A2})}{(X_2 + X_{A2})^2 + r_2^2}, \tag{2}$$

where $X_2 = \omega L_2 - 1/\omega C_2$. As shown in (1) and (2), Z_{ref} is dependent on X_{A2}, which can be controlled by the ATAC.
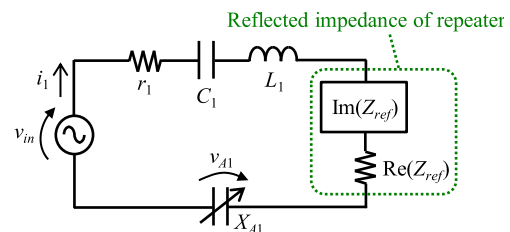

FIGURE 7. Equivalent circuit of Fig. 6 with reflected impedance.

The maximum repeater coil current can be achieved when $\text{Re}(Z_{ref})$ consumes the maximum power. According to the equivalent circuit shown in Fig. 7, the following conditions are required on X_{A1} and X_{A2}:

1. The reactance X_{A1} should be adjusted such that the total reactance of Fig. 7 should be zero, i.e. $X_{A1} = -\omega L_1 + 1/\omega C_1 - \text{Im}(Z_{ref})$.
2. The reactance X_{A2} should be adjusted such that the resistance $\text{Re}(Z_{ref})$ is equal if impossible, or at least close to r_1. Because $(X_2 + X_{A2})^2 \geq 0$, $\text{Re}(Z_{ref})$ must be equal to or smaller than $\omega^2 M^2 / r_2$. Therefore, X_{A2} should be adjusted such that $\text{Re}(Z_{ref}) = r_1$ if $\omega^2 M^2 / r_2 \geq r_1$, otherwise X_{A2} should be adjusted to satisfy $X_2 + X_{A2} = 0$.

The relation $\omega^2 M^2 / r_2 \geq r_1$ can be rewritten as $k \geq 1/(Q_1 Q_2)^{1/2}$, where k is the coupling coefficient defined as $k = M/(L_1 L_2)^{1/2}$; Q_1 and Q_2 are the quality factors of the transmitter and repeater, respectively, defined as $Q_1 = \omega L_1/r_1$ and $Q_2 = \omega L_2/r_2$. Therefore, the second condition indicates that X_{A2} should be adjusted such that $\text{Re}(Z_{ref}) = r_1$,

if $k \geq 1/(Q_1 Q_2)^{1/2}$; otherwise X_{A2} should be adjusted to satisfy $X_2 + X_{A2} = 0$. In addition, the inequality $k \geq 1/(Q_1 Q_2)^{1/2}$ is known as the condition in which the frequency splitting phenomenon occurs in a two-coil RIC-WPT system [18], [20]. Therefore, $\mathrm{Re}(Z_{ref}) = r_1$ can be achieved when the frequency splitting phenomenon occurs between the transmitter and the repeater.

In the proposed WPT systems, the ATACs are autonomously controlled to satisfy the aforementioned two conditions. As a result, the amplitude of the repeater coil current is controlled at its maximum possible value against the variation of resonant frequency and the magnetic coupling intensity. The next subsection discusses the phase angle of the gating signals to be set for these ATACs and the resultant repeater and transmitter coil current in the steady-state.

As discussed in the previous subsection, the reactance X_{A1} and X_{A2} should be negative because the ATACs should be operated as variable capacitors for the ZVS turn-on of the ATAC. Therefore, the proposed WPT system should be designed such that the reactance of the transmitter resonator excluding the ATAC1 but including the reflected reactance of the repeater, i.e. $\omega L_1 - 1/\omega C_1 + \mathrm{Im}(Z_{ref})$, is always inductive, and that the reactance of the repeater resonator excluding the ATAC2, i.e. $\omega L_2 - 1/\omega C_2$, is inductive as well.

D. OPERATION ANALYSIS

The analysis of the phase angle differences of the ATACs is performed based on the phasor diagram shown in Fig. 8, where V_{in}, V_{ind}, V_{A1}, V_{A2}, I_1 and I_2 are the root-mean-square values of the fundamental waves of v_{in}, v_{ind}, v_{A1}, v_{A2}, i_1 and i_2, respectively.
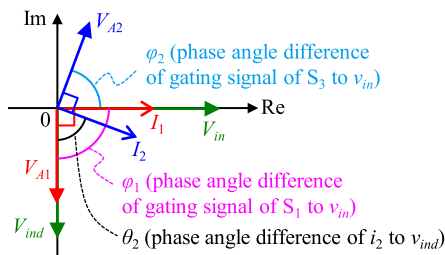
FIGURE 8. Phasor diagram related to ATACs in proposed WPT system.

According to the first condition discussed in previous section, the ac current of the transmitter coil should accurately be in phase with the ac voltage source. This requires that the phase angle difference φ_1 is set at $-\pi/2$ because the ac current flowing into the ATAC must have the phase difference of $\pi/2$ to the gate signal S_1 of ATAC1. Therefore, ATAC1 should be operated at the fixed phase angle difference, i.e., $\varphi_1 = -\pi/2$.

Meanwhile, the second condition discussed in previous section requires active control of the phase angle difference of ATAC2 depending on the coupling factor k. According to this condition, $\mathrm{Re}(Z_{ref})$ should be adjusted at r_1, if $k \geq 1/(Q_1 Q_2)^{1/2}$; otherwise $X_2 + X_{A2}$ should maintained at 0.

Hence, $\mathrm{Re}(Z_{ref}) = r_1$ can be developed as

$$\left(\frac{X_2 + X_{A2}}{r_2} \right)^2 = \frac{\omega^2 M^2}{r_1 r_2} - 1 = k^2 Q_1 Q_2 - 1, \qquad (3)$$

the phase angle difference θ_2 between I_2 and V_{ind} can be determined when $k \geq 1/(Q_1 Q_2)^{1/2}$ as

$$\theta_2 = \pm \tan^{-1} \left(\frac{X_2 + X_{A2}}{r_2} \right) = \pm \tan^{-1} \sqrt{k^2 Q_1 Q_2 - 1}. \quad (4)$$

$(-\pi/2 < \theta_2 < \pi/2$ because r_2 is positive.) Meanwhile, in the case of $k < 1/(Q_1 Q_2)^{1/2}$, the ATAC should entirely cancel the reactance of the repeater resonator X_2. Consequently, θ_2 is determined for $k < 1/(Q_1 Q_2)^{1/2}$ as

$$\theta_2 = 0. \qquad (5)$$

Because the ATAC1 ensures the transmitting coil current is in phase with the ac voltage source, voltage induction in the repeater coil has a phase difference of $\mathrm{sgn}(M)\pi/2$ with respect to the ac voltage source, where $\mathrm{sgn}(M)$ equals 1, if the mutual inductance M is positive. Otherwise, $\mathrm{sgn}(M)$ equals -1. Consequently, the phase angle difference of φ_2 can be determined as

$$\varphi_2 = \mathrm{sgn}(M)\, \pi \big/ 2 + \theta_2 - \pi \big/ 2. \qquad (6)$$

The resultant I_1 and I_2 can be obtained by calculating the phase angle differences φ_1 and φ_2. Because I_1 is in phase with V_{in}, $I_1 = V_{in}/\{r_1 + \mathrm{Re}(Z_{ref})\}$. Therefore,

$$I_1 = \begin{cases} \dfrac{V_{in}}{2r_1}, & \text{if } k\sqrt{Q_1 Q_2} \geq 1. \\[2mm] \dfrac{V_{in}}{r_1\left(1 + k^2 Q_1 Q_2\right)}, & \text{if } k\sqrt{Q_1 Q_2} < 1. \end{cases} \qquad (7)$$

Notably, when $V_{ind} = |\omega M| I_1$, the following relation is obtained.

$$V_{ind} = |\omega M|\, I_1 = k I_1 \sqrt{Q_1 Q_2} \sqrt{r_1 r_2}. \qquad (8)$$

Consequently, I_2 can be obtained as

$$I_2 = \begin{cases} \dfrac{V_{in}}{2\sqrt{r_1 r_2}}, & \text{if } k\sqrt{Q_1 Q_2} \geq 1. \\[2mm] \dfrac{k\sqrt{Q_1 Q_2}}{1 + k^2 Q_1 Q_2} \dfrac{V_{in}}{\sqrt{r_1 r_2}}, & \text{if } k\sqrt{Q_1 Q_2} < 1. \end{cases} \qquad (9)$$

As shown in (9), the repeater coil current is independent of the reactance of the resonators, i.e., $\omega L_2 - 1/\omega C_2$. Therefore, the proposed WPT system can stabilize the repeater coil current against the variation in the resonant frequency of the transmitter and repeater resonators. Certainly, I_2 is dependent on the quality factor of the transmitter and repeater resonators. However, these factors are far less sensitive to the variation in the resonant frequency compared with the reactance of the resonators. Additionally, the repeater coil current is independent of the magnetic coupling coefficient k when k is sufficiently large to cause the frequency splitting phenomenon. Therefore, the proposed WPT system can also stabilize the repeater coil current against the frequency splitting phenomenon at a large magnetic coupling intensity,

which affects the repeater coil current owing to the variation in the magnetic coupling intensity.

According to (4) and (6), two optimal values exist for φ_2 to maximize the amplitude of the repeater current in the case of $k \geq 1/(Q_1 Q_2)^{1/2}$. These two values of φ_2 result in opposite signs of the phase angle difference θ_2. Nonetheless both of φ_2 does not affect the amplitudes of I_1 and I_2. When k is close to the unity, the two optimal φ_2 approaches to $\pm \pi/2$, which indicates that the phase difference between i_1 and i_2 is 0 or π. Therefore, the two optimal φ_2 corresponds to the even and odd modes under the frequency splitting phenomenon.

As the dc voltage is stored in the smoothing capacitor of the ATAC, this voltage should be estimated for the practical design of the ATAC. Therefore, the amplitude of the ATAC output voltage V_{A1} and V_{A2} are calculated. Because V_{A1} and V_{A2} are identical to the voltage drop across the equivalent reactance X_{A1} and X_{A2}, respectively, $V_{A1} = X_{A1} I_1$ and $V_{A2} = X_{A2} I_2$. The reactance X_{A2} when $k \geq 1/(Q_1 Q_2)^{1/2}$ and $\theta_2 = \pm \tan^{-1}(k^2 Q_1 Q_2 - 1)^{1/2}$ can be calculated from (3) and (4) as

$$X_{A2} = -X_2 \pm r_2 \sqrt{k^2 Q_1 Q_2 - 1}. \qquad (10)$$

Therefore, Im(Z_{ref}) can be calculated as

$$\text{Im}\left(Z_{ref}\right) = \begin{cases} \mp r_1 \sqrt{k^2 Q_1 Q_2 - 1}, & \text{if } k\sqrt{Q_1 Q_2} \geq 1, \\ 0, & \text{if } k\sqrt{Q_1 Q_2} < 1. \end{cases} \qquad (11)$$

Consequently, V_{A1} is obtained as

$$V_{A1} = \begin{cases} \left| \omega L_1 - \frac{1}{\omega C_1} \mp r_1 \sqrt{k^2 Q_1 Q_2 - 1} \right| \frac{V_{in}}{2r_1}, \\ \quad \text{if } k\sqrt{Q_1 Q_2} \geq 1, \\ \left| \omega L_1 - \frac{1}{\omega C_1} \right| \frac{V_{in}}{r_1 (1 + k^2 Q_1 Q_2)}, \\ \quad \text{if } k\sqrt{Q_1 Q_2} < 1. \end{cases} \qquad (12)$$

Similarly, V_{A2} is obtained as

$$V_{A2} = \begin{cases} \left| \omega L_2 - \frac{1}{\omega C_2} \mp r_2 \sqrt{k^2 Q_1 Q_2 - 1} \right| \frac{V_{in}}{2\sqrt{r_1 r_2}}, \\ \quad \text{if } k\sqrt{Q_1 Q_2} \geq 1, \\ \left| \omega L_2 - \frac{1}{\omega C_2} \right| \frac{k\sqrt{Q_1 Q_2} V_{in}}{\sqrt{r_1 r_2}(1 + k^2 Q_1 Q_2)}, \\ \quad \text{if } k\sqrt{Q_1 Q_2} < 1. \end{cases} \qquad (13)$$

Because V_{A1} and V_{A2} are the root-mean-square values of the fundamental waves, the dc voltage V_{A1_dc} and V_{A2_dc} of the smoothing capacitors of ATAC1 and ATAC2 are obtained as

$$V_{A1\_dc} = \frac{\pi}{\sqrt{2}} V_{A1}, \quad V_{A2\_dc} = \frac{\pi}{\sqrt{2}} V_{A2}. \qquad (14)$$

As shown in (12)–(14), the necessary voltage tolerance of the smoothing capacitor of the ATAC increases as the reactance of the LC resonator increases and as the coupling coefficient increases or decreases. Therefore, a high voltage tolerance is required if the ATAC needs to compensate for a wide variation in resonant frequency and magnetic coupling intensity.

III. AUTONOMOUS CONTROL STRATEGY OF PROPOSED WIRELESS POWER TRANSFER SYSTEM

As previously discussed, the ATACs of the proposed WPT system should operate with an appropriate phase angle difference from the ac voltage source generated by the inverter of the transmitter. This section discusses a basic concept of the autonomous controller. The actual circuit for this controller is beyond the scope of this paper and will be investigated in a future study. However, the appropriateness of this concept was tested through experiment by manually controlling the proposed WPT system.

Fig. 9 illustrates the proposed WPT system with an autonomous controller. The controller comprises three parts: 1. The transmitter controller, which controls the inverter and ATAC1; 2. The repeater controller, which generates the control signal for the ATAC2; 3. A wireless communicator, which transmits the signal that synchronizes the inverter output voltage to the ATAC controller of the repeater.
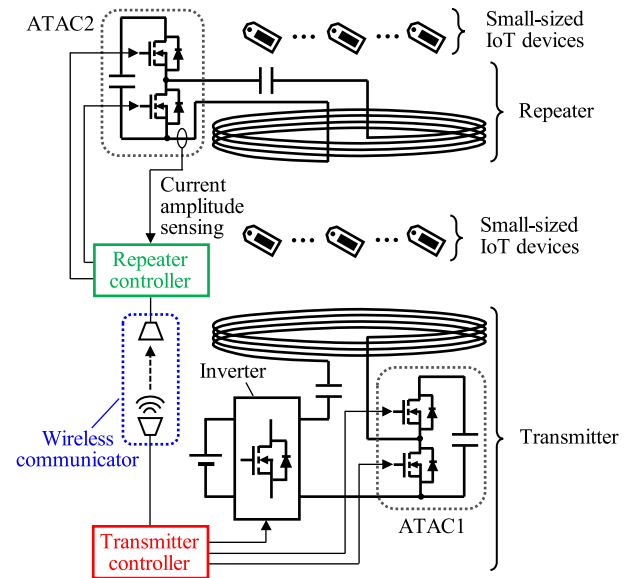
FIGURE 9. Concept of proposed WPT system with autonomous controller.

The transmitter controller generates the control signals of the inverter, determining the phase angle of the ac voltage output of the inverter. Meanwhile, the transmitter controller also generates the gating signals of the switching devices of ATAC1. As earlier mentioned, the ATAC1 should operate so that the phase angle of v_{A1} is delayed by $\pi/2$ relative to v_{in}. Thus, feedback control is not necessary for the transmitter controller because the ATAC1 operates at a fixed phase angle. Therefore, the gating signals for ATAC 1 can be simply generated by shifting the gating signals of the switching devices of the inverter by using a fixed phase delay circuit for example.

The wireless communicator transmits the signals synchronizing the inverter output voltage to the ATAC2 controller via a wireless connection. Although the practical design of the wireless communicator is out of scope of this paper, the most convenient signals for this synchronizing signal may be

the gating signals for the inverter. Any media can be utilized for the wireless connection. For example, infrared on-off keying communication [14] may be a convenient method for the WPT system with an operating frequency below approximately 10MHz.

The repeater controller generates the gating signals for the switching devices of ATAC2 based on the synchronization signal received from the wireless communicator. These gating signals are generated by shifting the received synchronization signal by an appropriate phase angle. According to the previous section, this phase angle can vary depend on the magnetic coupling coefficient k, which is often unknown particularly the position of the repeater is variable. In this case, the controller should search for the phase angle.

A simple method for searching for the appropriate phase angle is the perturbation and observation (P&O) method [14], [30]. Fig. 10 shows an example algorithm, which iteratively searches for the phase angle difference η between the high-side switch of ATAC2 and the synchronization signal by repeating small updates of η, based on the observation of the amplitude of the repeater coil current. For simplicity, the synchronizing signal is assumed to have no phase angle difference from the inverter output voltage, although a similar algorithm can be used when the signal has a phase angle difference. In Fig. 10, n is the index of the newest observation result; $I_{m2,n}$ is the observed repeater current amplitude; and $\Delta\eta$ is a predetermined small fixed phase angle value, which is added or subtracted to slightly change the current phase angle η to shift the synchronization signal. By repeating the update process of η, η converges into the appropriate value, resulting in adaptive maximization of the repeater current.
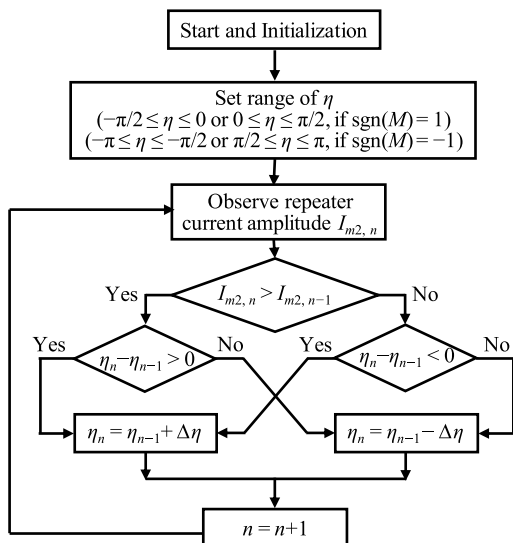

FIGURE 10. Searching algorithm for appropriate phase angle difference of ATAC2.

In the initial state of the algorithm, the adjustable range of η is chosen depending on the sign of the mutual inductance M, which should be provided to the control system

by the designer of the WPT system. In particular, the range of η should be set as $0 \le \eta \le \pi/2$ or $-\pi/2 \le \eta \le 0$ if $\text{sgn}(M) = 1$, and $-\pi \le \eta \le \pi/2$ or $\pi/2 \le \eta \le \pi$ if $\text{sgn}(M) = -1$. Two possible ranges for each sign of M correspond to even and odd mode operations when the magnetic coupling intensity is strong. The designer of the WPT system can freely choose from these two modes by considering the preferable mode.

IV. EXPERIMENT

Experiments to evaluate the operating principles of the proposed WPT system were conducted. These experiments test the stable maximization of the repeater current with varying magnetic coupling and resonant frequency as well as the resultant improvement of the charging area to the receiver.

A. EXPERIMENTAL PROTOTYPE

The schematic of the prototype of the proposed WPT system used for this experiment is shown in Fig. 11. This prototype comprised one transmitter, one repeater, and two receivers. The transmitter and repeater incorporate the Litz wire coils with the same diameter and number of turns. These coils were separated by a vertical distance. W2 could be varied through nine vertical positions to test the dependence on the magnetic coupling intensity. Meanwhile, the receiver had a small coil of thin copper wire with a diameter of 0.16 mm wound on the cylindrical ferrite core (7H20 [31] manufactured by TDK Co., Ltd.). The diameter of the receiver coil was 10.0 mm, which was far smaller than the diameters of the transmitter and receiver coils. As shown in Fig. 11, the small-sized receiver coils were fixed concentrically 150 mm above and below the repeater coil to avoid overcomplicating the experiment. The half-bridge inverter was adopted to excite the transmitter resonator, where V_{in_dc} is the DC voltage of the inverter.
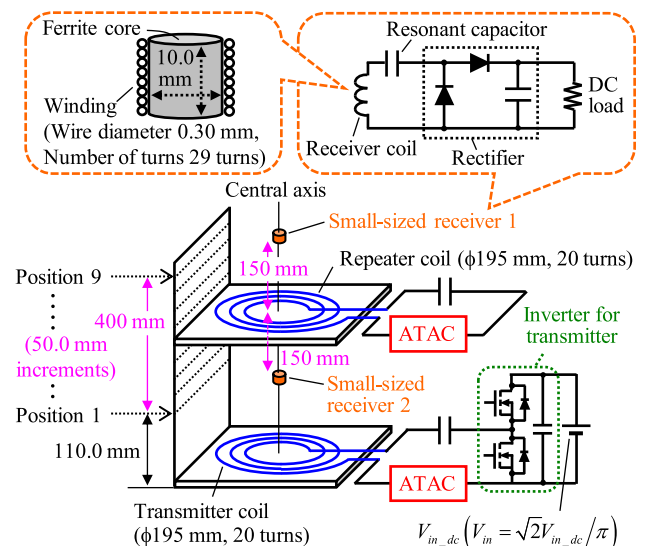

FIGURE 11. Schematic of the experimental setup for proposed system.

The photograph of the experimental setup of the proposed system is shown in Fig. 12. The gate control signals of the inverter and ATACs in this study were generated using a function generator. In addition, the power supplies for the gate drivers in the inverter and the ATACs were supplied using a common external power source. The operating phase angle of the ATAC in the repeater was adjusted to θ_{opt} using the function generator manually based on the flowchart in Fig. 10. In the experiment, the transmitter and repeater currents were measured using a current probe connected to an oscilloscope, while the DC voltages of the ATACs were measured using a digital multimeter.
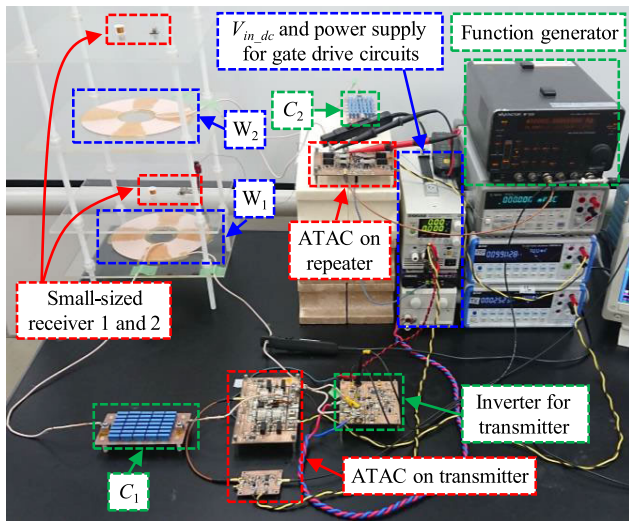

FIGURE 12. Photograph of the experimental setup for proposed system.

The circuit parameters of the proposed system and the system without the ATACs (i.e., the conventional system) are listed in Table 1. The operating frequency was set to 400.0 kHz for simplicity of the experimental system construction and waveform measurements, although the proposed system does not impose any requirement for the operating frequency. Because C_1 and C_2 for each system differ, r_1 and r_2 also differ from each system (r_1 includes the on-resistance of the power devices in the inverter.). In the conventional system, C_1 and C_2 were determined such that the resonant frequencies of the transmitter and repeater were equal to the operating frequency. However, C_1 and C_2 of the proposed system were determined based on (12) and (13) such that the phase difference angle between v_{A1} and i_1 as well as between v_{A2} and i_2 satisfy the condition that each ATAC achieves ZVS turn-on. Meanwhile, C_{r1} and C_{r2} were designed so that the resonant frequency of each receiver was close to the operating frequency. In addition, R_{dc1} and R_{dc2} of the receivers were designed with values in which each receiver can obtain the most output power when the transmitter and repeater currents are approximated to be uninfluenced by the receiver current. In the case of the conventional system, the output terminals of the ATACs were shorted when measuring the transmitter and repeater current, thereby eliminating the effect of the ATACs.

TABLE 1. Circuit parameters for experiments.

	Symbols / Parameters	Values
	Common circuit parameters	
L_1	Self-inductance of W_1	55.690 μH
L_2	Self-inductance of W_2	55.463 μH
C_{A1}	Capacitance of ATAC on transmitter	22 μF
C_{A2}	Capacitance of ATAC on repeater	22 μF
L_{r1}	Self-inductance of coil for receiver 1	23.360 μH
L_{r2}	Self-inductance of coil for receiver 2	23.889 μH
C_{r1}	Capacitance of receiver 1	6.777 nF
C_{r1}	Capacitance of receiver 2	6.627 nF
r_{r1}	Parasitic resistance of receiver 1	1.991 Ω
r_{r2}	Parasitic resistance of receiver 2	1.922 Ω
R_{dc1}	Output DC load resistance in receiver 1	9.813 Ω
R_{dc2}	Output DC load resistance in receiver 2	9.502 Ω
f_s	Operating frequency	400.00 kHz
V_{in_dc}	Input DC voltage	6.0 V
	Conventional system	
r_1	Parasitic resistance of transmitter	0.436 Ω
r_2	Parasitic resistance of transmitter	0.392 Ω
C_1	Capacitance of transmitter	2.844 nF
C_2	Capacitance of repeater	2.858 nF
	Proposed system ($0 \leq \theta \leq \pi/2$)	
r_1	Parasitic resistance of transmitter	0.429 Ω
r_2	Parasitic resistance of transmitter	0.387 Ω
C_1	Capacitance of transmitter	3.092 nF
C_2	Capacitance of repeater	3.086 nF
	Proposed system ($-\pi/2 \leq \theta \leq 0$)	
r_1	Parasitic resistance of transmitter	0.416 Ω
r_2	Parasitic resistance of transmitter	0.367 Ω
C_1	Capacitance of transmitter	3.281 nF
C_2	Capacitance of repeater	3.258 nF

B. STABILITY AGAINST VARIATION IN MAGNETIC COUPLING INTENSITY

Here, we validate that the repeater current of the proposed system can be obtained stably with varying magnetic coupling intensity. In particular, we compared the repeater current between the conventional and proposed systems when the position of W_2 changed. The coupling coefficient k between the transmitter and repeater coils in each position of the repeater coil is shown in Fig. 13. The evaluation was performed as a representative example only when the coupling coefficient M was positive. In the experiment, the small-seized receivers were excluded because this subsection aims to evaluate the repeater current stability with varying magnetic coupling intensity between W_1 and W_2.

The experimental and analytical calculation results of I_2, I_1, V_{A1_dc}, and V_{A2_dc} when $0 \leq \varphi_2 \leq \pi/2$ and $-\pi/2 \leq \varphi_2 \leq 0$ are shown in Figs. 14 and 15, respectively. The results of I_1 and I_2 of the conventional system in Figs. 14 and 15 are the same. Here, we excluded the detailed derivation processes
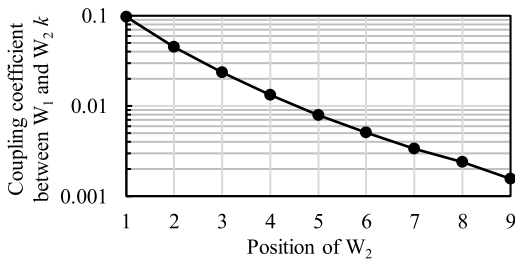
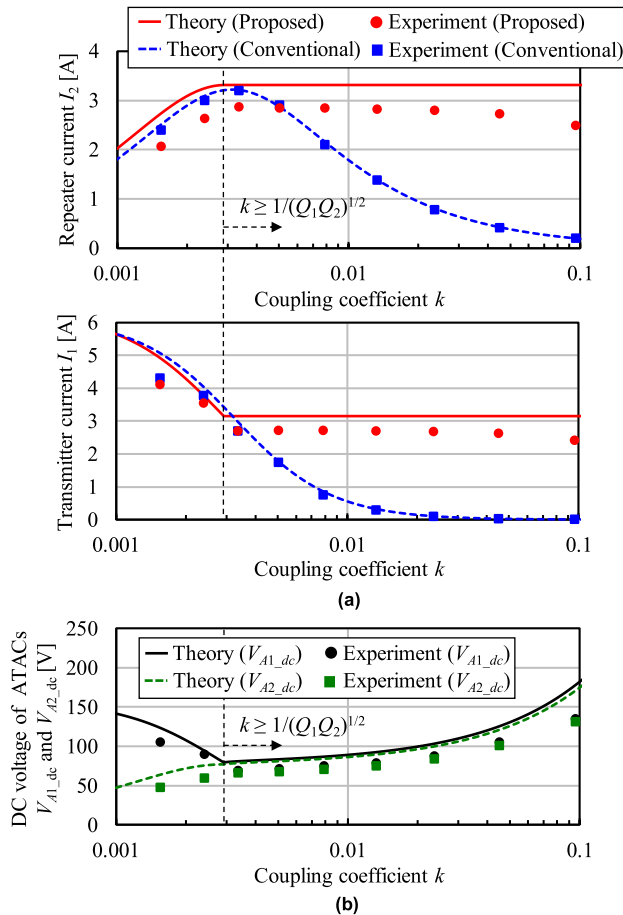**FIGURE 13.** Coupling coefficient between W_1 and W_2 at each position of W_2.

FIGURE 14. Characteristics against variation in magnetic coupling intensity when $0 \leq \varphi_2 \leq \pi/2$. (a) Resonator current. (b) DC voltage of ATAC.
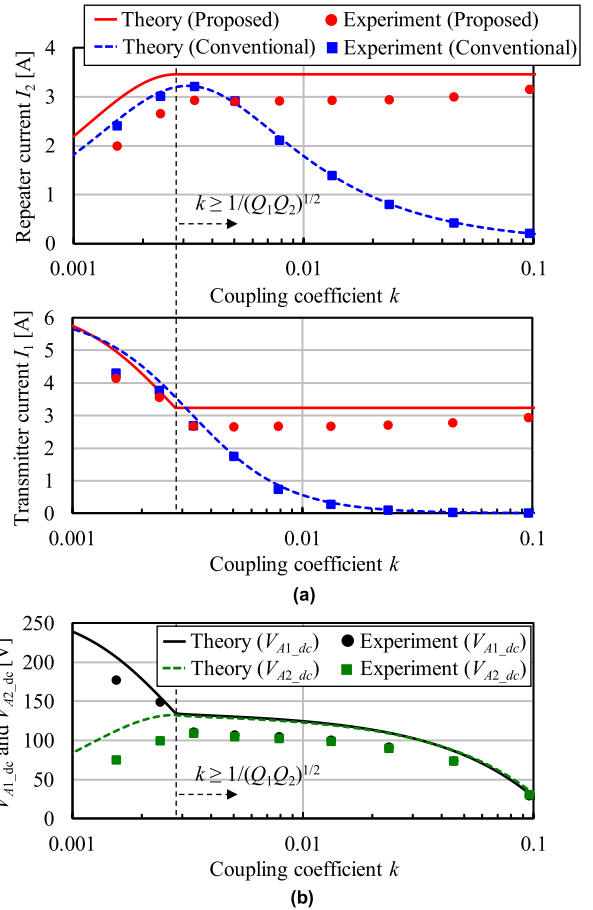

FIGURE 15. Characteristics against variation in magnetic coupling intensity when $-\pi/2 \leq \varphi_2 \leq 0$. (a) Resonator current. (b) DC voltage of ATAC.

of the theoretical calculation results of I_1 and I_2 in the conventional system because the currents in the WPT system consisting of two resonators have already been studied [6]. As shown in Figs. 14 and 15, I_2 of the conventional system is significantly changed when $k \geq 1/(Q_1 Q_2)^{1/2}$ owing to the frequency splitting phenomenon. In contrast, the proposed system can obtain an approximately constant large current when $k \geq 1/(Q_1 Q_2)^{1/2}$ regardless of the coupling coefficient. However, the I_2 of both systems decreased as k decreased when $k < 1/(Q_1 Q_2)^{1/2}$. When $k < 1/(Q_1 Q_2)^{1/2}$, the rate of

decrease of I_2 owing to a decrease in k is almost the same between the proposed and conventional systems. Therefore, the proposed system can stabilize the repeater current with varying magnetic coupling intensity.

However, as shown in Figs. 14 and 15, an error exists between the experimental and analytical calculation results of the proposed system. This error results from slight losses in the ATACs. Although the ATACs can achieve ZVS turn-on, they still have conduction, turn-off, printed circuit board, and reverse conduction losses. These losses are slight; however, they easily influence experimental results, owing to the large quality factors of the transmitter and repeater resonators used in this experiment. Although the ATAC causes losses, the proposed system can significantly improve the repeater current stability with varying magnetic coupling intensity with only a slight increase in losses.

C. STABILITY AGAINST VARIATION IN RESONANT FREQUENCY

Subsequently, we validated that the repeater current of the proposed system can be obtained stably with variation in the resonant frequency. We compared the repeater current
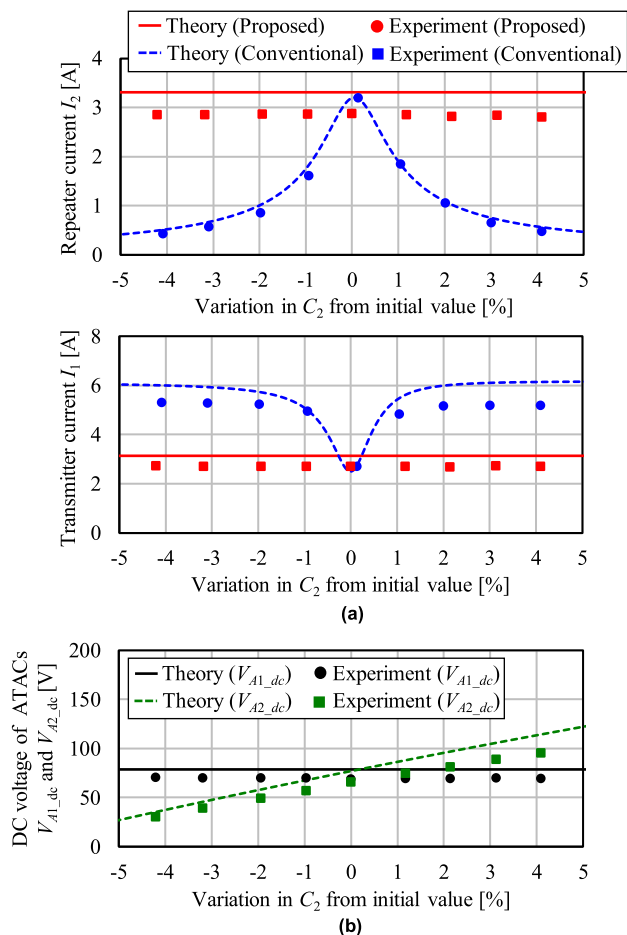
FIGURE 16. Characteristics against variation in resonant frequency when $0 \le \varphi_2 \le \pi/2$. (a) Resonator current. (b) DC voltage of ATAC.

FIGURE 17. Characteristics against variation in resonant frequency when $-\pi/2 \le \varphi_2 \le 0$. (a) Resonator current. (b) DC voltage of ATAC.

when C_2 changed by $\pm 5\%$ from the designed value between the proposed and conventional systems. The repeater was fixed at position 7. Furthermore, similar to the previous subsection, the small-seized receivers were removed in this experiment.

The experimental and analytical calculation results of I_2, I_1, V_{A1_dc}, and V_{A2_dc} when $0 \le \varphi_2 \le \pi/2$ and $-\pi/2 \le \varphi_2 \le 0$ are shown in Figs. 16 and 17, respectively. The results of I_2 for the conventional system in Figs 16 and 17 are similar. In the conventional system, the repeater current significantly decreases when C_2 varies from the designed value. However, the proposed system can achieve a constant repeater current regardless of the variation in C_2 because the ATAC on the repeater compensates for the effect of the variation in C_2. Therefore, the proposed system can stabilize the repeater current with variation in the resonant frequency of the repeater. Although we excluded the experimental results, the proposed system can also compensate for the variation in the resonant frequency of the transmitter resonator because the ATAC on the transmitter automatically cancels all reactance in the transmitter, as discussed in Section II.
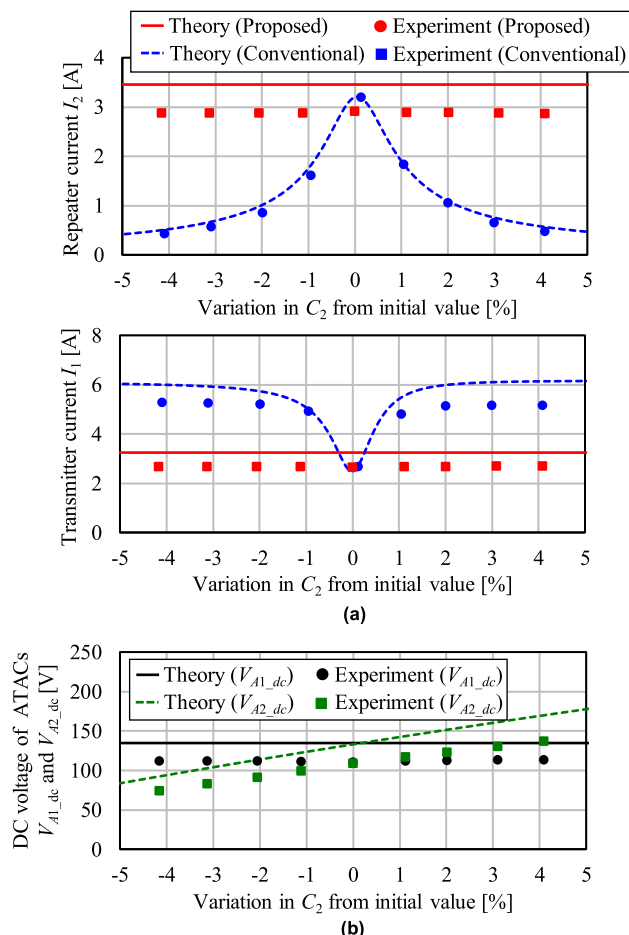
D. EXPANSION OF CHARGING AREA

Finally, we validated the proposed system's ability to improve the charging area of small-sized receivers compared with the conventional system. We compared the output power of the small-sized receiver of the proposed and conventional systems when the position of W_2 was set to positions 4, 5, and 6. The coupling coefficients between the corresponding coils are shown in Fig. 18, where W_{ri} ($i = 1, 2$) represent receiver coils. Moreover, this section indicates the difference in the output power depending on the range of φ_2, i.e., $0 \le \varphi_2 \le \pi/2$ and $-\pi/2 \le \varphi_2 \le 0$.

The experimental results of the output power in Receiver 1 are shown in Fig. 19 (a). Notably, the output power of each receiver was measured separately for Receiver 1 and Receiver 2 (the receiver coil on the side not being measured was opened). Furthermore, the operating waveforms of the proposed system when the position of W_2 was set to Position 6 and the output power of Receiver 1 was measured are shown in Fig. 20. The output power of Receiver 1 in the conventional system is almost equivalent to that of the
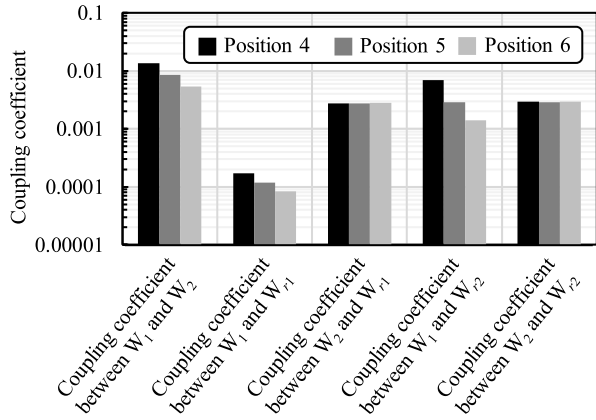
FIGURE 18. Coupling coefficient between corresponding coils at each position of W$_2$.
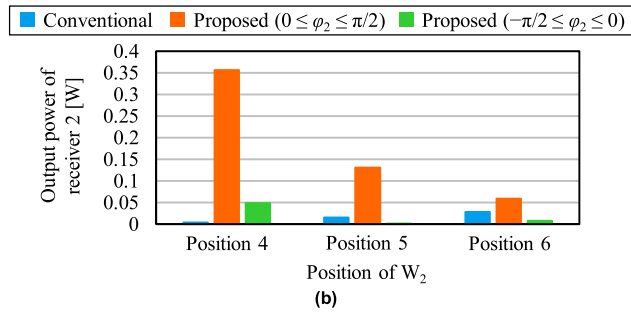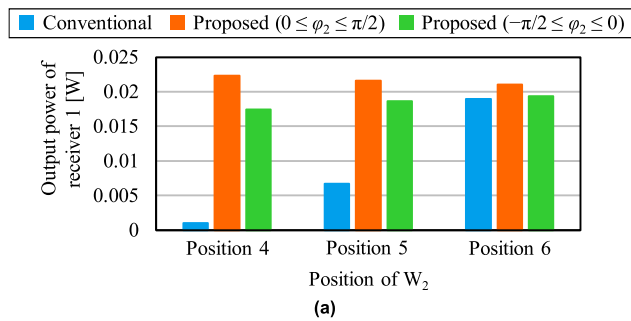

FIGURE 19. Output power of each receiver. (a) Receiver 1. (b) Receiver 2.

FIGURE 20. Operating waveforms of proposed system when W$_2$ was set to position 6 and receiver 1 was measured. (a) $0 \leq \varphi_2 \leq \pi/2$. (b) $-\pi/2 \leq \varphi_2 \leq 0$.

proposed system when W$_2$ was set to Position 6. However, the output power decreased significantly as the distance between W$_1$ and W$_2$ decreased because the repeater current decreased owing to the frequency splitting phenomenon. However, the output power of the proposed system was almost constant because the repeater current was almost constant regardless of the position of the repeater coil. However, when the distance between W$_1$ and W$_2$ decreased, the output power of the proposed system changed slightly owing to the magnetic field generated by the transmitter. For $0 \leq \varphi_2 \leq \pi/2$, as the distance between W$_1$ and W$_2$ decreased, the phase angle difference between the repeater current i_2 and transmitter current i_1 approached 0. Therefore, the magnetic field resulting from the transmitter current and that resulting from the repeater current strengthen each other. In contrast, when $-\pi/2 \leq \varphi_2 \leq 0$, the phase angle difference between the
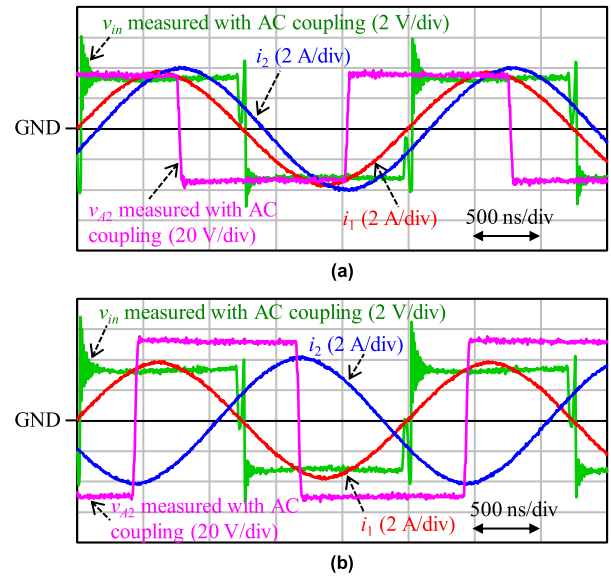
repeater current i_2 and transmitter current i_1 approached π as the distance between W$_1$ and W$_2$ decreased, as shown in Fig. 20 (b). Hence, the magnetic field resulting from the transmitter current weakens the magnetic field generated by the repeater current. Thus, in the proposed system, the output power of Receiver 1 when $0 \leq \varphi_2 \leq \pi/2$ is larger than when $-\pi/2 \leq \varphi_2 \leq 0$ as the distance between W$_1$ and W$_2$ decreased.

Then, the experimental results of the output power in Receiver 2 are shown in Fig. 19 (b). Similar to Fig. 19 (a), the output power of Receiver 2 in the conventional system decreased as the distance between W$_1$ and W$_2$ decreased because the transmitter and repeater currents were significantly reduced by the frequency splitting phenomenon. Hence, in the case of the proposed system when $0 \leq \varphi_2 \leq \pi/2$, the output power was larger than the others. This is because the proposed system can stabilize the repeater current regardless of the variations in the magnetic coupling intensity and also the phase angle difference between the repeater current i_2 and the transmitter current i_1 approached zero. However, in the case of the proposed system, when $-\pi/2 \leq \varphi_2 \leq 0$, the output power of Receiver 2 placed between the transmitter and repeater coils was significantly lower than that when $0 \leq \varphi_2 \leq \pi/2$. This is because the phase angle difference between the repeater current i_2 and the transmitter current i_1 approached π and the transmitter and repeater currents weakened the magnetic field of each other. Therefore, the proposed system for $0 \leq \varphi_2 \leq \pi/2$ is the best in terms of the provision of a wide charging area. In the experiments of this section, the distance between the repeater and each receiver is fixed. Nevertheless, we believe that the proposed system for $0 \leq \varphi_2 \leq \pi/2$ tends to obtain more output power than the conventional system at different distances between the

repeater and the receiver. This is because the experiments in Section IV-B have demonstrated that the proposed system can achieve more stable repeater current amplitudes with respect to the coupling coefficient than the conventional system.

V. CONCLUSION

This paper proposed a novel RIC-WPT system and its control strategy that can stabilize the repeater current regardless of variations in the resonant frequency and magnetic coupling intensity to expand the charging area for small-sized receivers. The proposed WPT system had ATACs in the transmitter and repeater to actively adjust the resonant frequency of each resonator. The control for the ATAC of the transmitter was simple because it is driven by the fixed phase angle. The ATAC in the repeater dynamically adjusted the phase angle of the output voltage of the ATAC to maximize the repeater current based on the P&O method. From the experimental results in Figs. 14-17, it was verified that the proposed WPT system could stabilize the repeater current even when the position of the repeater coil and the resonant frequency of the repeater changed. Furthermore, it was verified that the proposed WPT system effectively expanded the charging area of small-sized receivers as demonstrated in Fig. 19. From these results, we validated the feasibility and effectiveness of the proposed reactance compensator. Therefore, the proposed WPT system is promising as a practical method to provide a wide charging area for small-sized receivers.

REFERENCES

[1] P. Pérez-Nicoli, A. Rodríguez-Esteva, and F. Silveira, "Bidirectional analysis and design of RFID using an additional resonant coil to enhance read range," *IEEE Trans. Microw. Theory Techn.*, vol. 64, no. 7, pp. 2357–2367, Jul. 2016.

[2] E. S. Lee, J. S. Choi, H. S. Son, S. H. Han, and C. T. Rim, "Six degrees of freedom wide-range ubiquitous IPT for IoT by DQ magnetic field," *IEEE Trans. Power Electron.*, vol. 32, no. 11, pp. 8258–8276, Nov. 2017.

[3] R. Narayanamoorthi and A. V. Juliet, "IoT-enabled home cage with three-dimensional resonant wireless power and data transfer scheme for freely moving animal," *IEEE Sensors J.*, vol. 18, no. 19, pp. 8154–8161, Oct. 2018.

[4] Y. Gao, M. Fu, H. Wang, and J. Liang, "A 2-D inductive power transfer network for powering massive neighboring IoT devices," *IEEE Access*, vol. 10, pp. 113560–113569, 2022.

[5] K. Umetani, T. Honjo, T. Koyama, M. Ishihara, and E. Hiraki, "Receiving-coil structure reducing stray AC resistance for resonant coupling wireless power transfer," *IET Power Electron.*, vol. 12, no. 9, pp. 2338–2344, Aug. 2019.

[6] M. Ishihara, K. Umetani, and E. Hiraki, "Strategy of topology selection based on quasi-duality between series–series and series–parallel topologies of resonant inductive coupling wireless power transfer systems," *IEEE Trans. Power Electron.*, vol. 35, no. 7, pp. 6785–6798, Jul. 2020.

[7] S. Mao, J. Zhang, K. Song, G. Wei, and C. Zhu, "Wireless power transfer using a field-enhancing coil and a small-sized receiver with low coupling coefficient," *IET Power Electron.*, vol. 9, no. 7, pp. 1546–1552, Jun. 2016.

[8] K. Lee and S. H. Chae, "Effect of quality factor on determining the optimal position of a transmitter in wireless power transfer using a relay," *IEEE Microw. Wireless Compon. Lett.*, vol. 27, no. 5, pp. 521–523, May 2017.

[9] K. Lee and S. H. Chae, "Power transfer efficiency analysis of intermediate-resonator for wireless power transfer," *IEEE Trans. Power Electron.*, vol. 33, no. 3, pp. 2484–2493, Mar. 2018.

[10] Y. Sun, Z.-J. Liao, Z.-H. Ye, C.-s. Tang, and P.-Y. Wang, "Determining the maximum power transfer points for MC-WPT systems with arbitrary number of coils," *IEEE Trans. Power Electron.*, vol. 33, no. 11, pp. 9734–9743, Nov. 2018.

[11] Q. Wang and Y. Wang, "Power efficiency optimisation of a three-coil wireless power transfer using compensatory reactance," *IET Power Electron.*, vol. 11, no. 13, pp. 2102–2108, Nov. 2018.

[12] M. Ishihara, K. Umetani, and E. Hiraki, "Impedance matching to maximize induced current in repeater of resonant inductive coupling wireless power transfer systems," in *Proc. IEEE Energy Convers. Congr. Expo. (ECCE)*, Portland, OR, USA, Sep. 2018, pp. 6194–6201.

[13] K. Fujiki, M. Ishihara, K. Umetani, and E. Hiraki, "Experimental verification of impedance matching method for repeater to improve spatial freedom of 6.78 MHz resonant inductive coupling wireless power transfer systems," in *Proc. 21st Eur. Conf. Power Electron. Appl. (EPE ECCE Eur.)*, Genova, Italy, Sep. 2019, pp. P.1–P.10.

[14] A. Konishi, K. Umetani, M. Ishihara, and E. Hiraki, "Autonomous resonant frequency tuner for a 6.78MHz inductive coupling wireless power transfer system to stably maximize repeater current," *IEEJ J. Ind. Appl.*, vol. 12, no. 2, pp. 215–227, Mar. 2023.

[15] H. L. Li, A. P. Hu, G. A. Covic, and C. S. Tang, "Optimal coupling condition of IPT system for achieving maximum power transfer," *Electron. Lett.*, vol. 45, no. 1, p. 76, 2009.

[16] H. H. Wu, A. P. Hu, S. C. Malpas, and D. M. Budgett, "Determining optimal tuning capacitor values of TET system for achieving maximum power transfer," *Electron. Lett.*, vol. 45, no. 9, p. 448, 2009.

[17] D.-W. Seo, J.-H. Lee, and H.-S. Lee, "Optimal coupling to achieve maximum output power in a WPT system," *IEEE Trans. Power Electron.*, vol. 31, no. 6, pp. 3994–3998, Jun. 2016.

[18] R. Huang, B. Zhang, D. Qiu, and Y. Zhang, "Frequency splitting phenomena of magnetic resonant coupling wireless power transfer," *IEEE Trans. Magn.*, vol. 50, no. 11, pp. 1–4, Nov. 2014.

[19] D.-W. Seo and J.-H. Lee, "Frequency-tuning method using the reflection coefficient in a wireless power transfer system," *IEEE Microw. Wireless Compon. Lett.*, vol. 27, no. 11, pp. 959–961, Nov. 2017.

[20] R. Huang and B. Zhang, "Frequency, impedance characteristics and HF converters of two-coil and four-coil wireless power transfer," *IEEE J. Emerg. Sel. Topics Power Electron.*, vol. 3, no. 1, pp. 177–183, Mar. 2015.

[21] A. Trigui, S. Hached, F. Mounaim, A. C. Ammari, and M. Sawan, "Inductive power transfer system with self-calibrated primary resonant frequency," *IEEE Trans. Power Electron.*, vol. 30, no. 11, pp. 6078–6087, Nov. 2015.

[22] J. Tian and A. P. Hu, "A DC-voltage-controlled variable capacitor for stabilizing the ZVS frequency of a resonant converter for wireless power transfer," *IEEE Trans. Power Electron.*, vol. 32, no. 3, pp. 2312–2318, Mar. 2017.

[23] J. Zhao, J. Zhang, and Y. Zhu, "A flexible wireless power transfer system with switch controlled capacitor," *IEEE Access*, vol. 7, pp. 106873–106881, 2019.

[24] L. Zhou, R. Mai, S. Liu, J. Yu, Y. Li, and L. Fu, "Minimizing input current of the rectifier of LCC–LCC compensated IPT systems by switch-controlled capacitor for improving efficiency," *IEEE Trans. Ind. Appl.*, vol. 58, no. 1, pp. 1010–1021, Jan. 2022.

[25] J. Li, J. Wang, J. Li, and J. Chen, "Multivariable coordinated control strategy for efficiency optimization without real-time wireless feedback communication in wireless power transfer," *IEEE Access*, vol. 10, pp. 55381–55395, 2022.

[26] Z. Zhang, W. Ai, Z. Liang, and J. Wang, "Topology-reconfigurable capacitor matrix for encrypted dynamic wireless charging of electric vehicles," *IEEE Trans. Veh. Technol.*, vol. 67, no. 10, pp. 9284–9293, Oct. 2018.

[27] Y. Lim, H. Tang, S. Lim, and J. Park, "An adaptive impedance-matching network based on a novel capacitor matrix for wireless power transfer," *IEEE Trans. Power Electron.*, vol. 29, no. 8, pp. 4403–4413, Aug. 2014.

[28] Y. Endo and Y. Furukawa, "Proposal for a new resonance adjustment method in magnetically coupled resonance type wireless power transmission," in *IEEE MTT-S Int. Microw. Symp. Dig.*, May 2012, pp. 263–266.

[29] L. Shi, P. Alou, J. Á. Oliver, J. C. Rodriguez, A. Delgado, and J. A. Cobos, "A self-adaptive wireless power transfer system to cancel the reactance," *IEEE Trans. Ind. Electron.*, vol. 68, no. 12, pp. 12141–12151, Dec. 2021.

[30] M. Fu, H. Yin, X. Zhu, and C. Ma, "Analysis and tracking of optimal load in wireless power transfer systems," *IEEE Trans. Power Electron.*, vol. 30, no. 7, pp. 3952–3963, Jul. 2015.

[31] *TDK Ferrite Cores for Transformer & Choke Coil*. Accessed: Jan. 9, 2023. [Online]. Available: https://www.es.co.th/Schematic/PDF/FDK-FERRITE.PDF

MASATAKA ISHIHARA (Member, IEEE) received the B.S. and M.S. degrees in electrical engineering from Shimane University, Matsue, Japan, in 2015 and 2017, respectively, and the Ph.D. degree in electrical engineering from Okayama University, Okayama, Japan, in 2021.

He is currently an Assistant Professor with Okayama University. His research interests include wireless power transfer systems, the design of integrated magnetic components, and wide bandgap (WBG) power semiconductor device modeling and driving.

Dr. Ishihara is a Member of the Institute of Electrical Engineers of Japan and the Japan Institute of Power Electronics.

KAZUHIRO UMETANI (Member, IEEE) received the M.S. and Ph.D. degrees in geophysical fluid dynamics from Kyoto University, Kyoto, Japan, in 2004 and 2007, respectively, and the second Ph.D. degree in electrical engineering from Shimane University, Matsue, Japan, in 2015.

From 2007 to 2008, he was a Circuit Design Engineer with Toshiba Corporation, Japan. From 2008 to 2014, he was with the Power Electronics Group, DENSO Corporation, Japan. From 2014 to 2020, he was an Assistant Professor with Okayama University, Okayama, Japan. From 2020 to 2021, he was an Associate Professor with Tohoku University, Miyagi, Japan. He is currently an Associate Professor with Okayama University. His research interests include new circuit configurations in power electronics and power magnetics for vehicular applications.

Dr. Umetani is a Member of the Institute of Electrical Engineers of Japan and the Japan Institute of Power Electronics.

AKIHIRO KONISHI (Member, IEEE) received the B.S. degree from the National Institute of Technology, Nara College (NITNC), Nara, Japan, in 2017, and the M.S. and Ph.D. degrees in electrical engineering from Okayama University, Okayama, Japan, in 2019 and 2023, respectively. He has been engaged as a Project Assistant Professor with Chiba University, Chiba, Japan, since 2023. His research interests include wireless power transfer systems and the design of a controller for a high-frequency switching circuit.

EIJI HIRAKI (Member, IEEE) received the M.Sc. and Ph.D. degrees in electrical engineering from Osaka University, Osaka, Japan, in 1990 and 2004, respectively.

He joined Mazda Motor Corporation, Hiroshima, Japan, in 1990. From 1995 to 2013, he was with the Power Electronics Laboratory, Yamaguchi University, Yamaguchi, Japan. He is currently a Professor with Okayama University, Okayama, Japan. His research interests include circuits and control systems of power electronics, particularly soft-switching techniques for high-frequency switching power conversion systems.

Dr. Hiraki is a Member of the Institute of Electrical Engineers of Japan and the Japan Institute of Power Electronics.

● ● ●